Journal of Magnetism and Magnetic Materials 473 (2019) 85–91

Contents lists available at ScienceDirect

Journal of Magnetism and Magnetic Materials

journal homepage: www.elsevier.com/locate/jmmm

Research articles

Influence of synthesis methods on structural and magnetic characteristics of Mg–Zn-ferrite nanopowders

E. Petrova[a], D. Kotsikau[a,*], V. Pankov[a], A. Fahmi[b]

[a] Department of Chemistry, Belarusian State University, 4 Nezavisimosti Av., 220030 Minsk, Belarus
[b] Rhine-Waal University of Applied Science, 47533 Kleve, Germany

ARTICLE INFO

Keywords:
A. Magnetic materials
A. Nanostructures
B. Chemical synthesis
D. Magnetic properties

ABSTRACT

Structural characteristics and magnetic properties of $Mg_xZn_{1-x}Fe_2O_4$ (x = 0.25; 0.5; 0.7) nanomaterials prepared by autocombustion, co-precipitation and spray pyrolysis methods were studied. Different characterization techniques are used to study the structural formation of the generated nanoparticles, namely X-ray diffraction (XRD), scanning (SEM) and transmission electron microscopy (TEM), infrared spectroscopy (FT-IR) and vibrating sample magnetometery (VSM). In case of citrate autocombustion and co-precipitation methods, the magnetization goes through a maximum at $Mg_{0.5}Zn_{0.5}Fe_2O_4$ composition, while the dependence on the composition is subtle for spray pyrolysis. An increase in temperature and duration of heat treatment during the synthesis process leads to a particle size growth and to a cation redistribution between spinel sub-lattices. These resulted in a significant increase in the specific magnetization of the particles generated by citrate autocombustion method. The nanoparticles synthesized by co-precipitation method exhibit superparamagnetic behavior with no coercivity at room temperature. Nonetheless, the materials prepared by spray pyrolysis and citrate autocombustion methods are found to possess small coercivity of 30–80 Oe. The highest specific magnetization at room temperature is referring to $Mg_{0.5}Zn_{0.5}Fe_2O_4$ nanoparticles obtained by citrate autocombustion method (30 emu/g). The revealed correlations can be used to synthesize spinel ferrite nanoparticles with well-defined collective properties for a wide spectrum of applications.

1. Introduction

Magnetic nano-sized ferrites are promising materials due to their unique properties essential for various applications, such as microwave and data storage devices, gas and humidity sensors, targeted drug delivery, magnetic hyperthermia, contrast agents for magnetic resonance imaging (MRI), bioseparation, etc. [1–4]. The magnetic properties of ferrites, namely magnetic saturation and coercivity are the key aspects in many of these applications. Possible ways to tailor the magnetic properties of ferrite materials are changing their composition by doping with ions of other metals and/or controlling their particle size. Both can be varied over a wide range by selecting the synthesis method and conditions.

The possibility of practical application of nanoparticles, however, is determined not only by their magnetic properties, but also by their toxicity, as well as by the cost of production. For example, nanoparticles of magnesium-zinc ferrites have been proposed as a low-toxic analog of nickel ferrite nanoparticles widely used in electronics [5]. Doping with small amounts of magnesium and zinc affects the magnetic properties of magnetite, which has a positive effect on the contrasting ability of MRI contrast agents [6]. Stoichiometric Mn–Zn-ferrites can be potentially used as materials for magnetic hyperthermia, for which their low toxicity is of great importance [7]. Therefore, they appear to be prospective research subjects.

Structural formula of spinel ferrite can be written as $(Me_{1-i}Fe_i)[Me_iFe_{2-i}O_4]$, where *Me* is divalent metallic ion, the parentheses represent the coordination of the tetrahedral sites (*A*-site), the square brackets – octahedral [*B*-site] sites, and *i* is called the inversion degree; i.e., the fraction of the *A*-sites occupied by Fe^{3+} ions. In case of magnesium-zinc ferrites, the magnetic moment of the material is determined only by the distribution of Fe^{3+} ions between *A*- and *B*-sublattices, since Zn^{2+} and Mg^{2+} ions are diamagnetic. The content ratio of doping ions will also matter, as Zn^{2+} ions tend to occupy *A*-sites and Mg^{2+} enters preferentially *B*-sites, and their distribution depends on synthesis conditions [8–11]. Classical methods to synthesize nanosized magnesium-zinc ferrites are co-precipitation [5,12,13], autocombustion

* Corresponding author.
E-mail addresses: petrovaeg@bsu.by (E. Petrova), kotsikau@bsu.by (D. Kotsikau), pankov@bsu.by (V. Pankov), amir.fahmi@hochschule-rhein-waal.de (A. Fahmi).

https://doi.org/10.1016/j.jmmm.2018.09.128
Received 21 June 2018; Received in revised form 20 September 2018; Accepted 30 September 2018
Available online 02 October 2018
0304-8853/

of organic precursors [14–17], mechanochemical sintering [18], etc.

In the present work, an influence of the preparation methods and the particular synthesis conditions on the structure and magnetic properties of $Mg_xZn_{1-x}Fe_2O_4$ ($x = 0.25$; 0.5; 0.7) nanoparticles obtained by citrate autocombustion, spray pyrolysis and co-precipitation methods has been studied. These methods were chosen since they have different temperature regimes and facilitate uniform nanoparticles generating with controllable diameters and a relatively narrow size distribution.

2. Experimental techniques.

2.1. Co-precipitation synthesis

A standard chemical co-precipitation method was used. The precursor solution was prepared by dissolving $Fe(NO_3)_3{\cdot}9H_2O$, $Mg(NO_3)_2{\cdot}6H_2O$ and $Zn(NO_3)_2{\cdot}6H_2O$ in deionized water with a molar ratio Fe : Mg : Zn = 2 : x : (1 − x). Sodium hydroxide taken in 10% excess to the stoichiometric value was used as a precipitant. The solution of salts was quickly transferred to alkali medium under stirring and heated to 90 °C for 30 min. The precipitate was washed several times in deionized water until pH reaches ~7, and dried at 40 °C in air.

2.2. Spray pyrolysis synthesis

Water solution of the precursors was obtained by dissolving Fe(III), Mg(II) and Zn(II) nitrates in deionized water with a molar ratio Fe : Mg : Zn = 2 : x : (1 − x) and NaCl taken in 5 : 1 wt ratio to the resulting ferrite. The presence of NaCl during the crystallization prevents the generated nanoparticles from aggregation in high temperature reaction zone. The solution was transformed into aerosol with an ultrasonic atomizer. The aerosol was then carried to the reaction zone of the furnace (T = 650 °C) with a nitrogen flow (flow rate is 5 L/min). The generated powder was collected in an electrostatic precipitator heated to 200 °C to prevent water condensation. Finally, NaCl additive was removed thoroughly from the powders by washing with deionized water using magnetic decantation method, and dried at 40 °C in air.

2.3. Citrate autocombustion synthesis

To prepare $Mg_xZn_{1-x}Fe_2O_4$ nanoparticles by sol-gel autocombustion method, $Mg(NO_3)_2{\cdot}6H_2O$, $Zn(NO_3)_2{\cdot}6H_2O$, $Fe(NO_3)_3{\cdot}9H_2O$ and citric acid ($C_6H_8O_7{\cdot}H_2O$) were dissolved in deionized water in a molar ratio of metal nitrates to citric acid taken as 1 : 3. Then, NaCl was added to the precursor solution in a weight ratio 5 : 1 for NaCl : product. The precursor solution was heated on a hot plate to evaporate the excess water until an auto-ignited combustion occurred. The product of the combustion in NaCl matrix was additionally heated for 3 h at 300 °C in air to remove the traces of carbon. Finally, NaCl was removed by washing with deionized water to obtain nanosized $Mg_xZn_{1-x}Fe_2O_4$ particles. The resulting powder was dried at 40 °C in air.

2.4. Characterization

X-ray diffraction (XRD) patterns of the powdered samples were recorded on a DRON-2.0 diffractometer (Co $K\alpha$-radiation) in the range 2θ = 20–80°. The lattice constants were refined using RTP 3.3 X-ray structure tabular processor. The average crystallite size (d_{XRD}) was estimated from the broadening of diffraction lines using the Scherrer equation, $d_{XRD} = k\lambda/[(B–b)\cos\theta]$, with the wavelength λ, the peak width B, the instrumental broadening b, the Bragg angle θ, and the shape factor $k \approx 0.90$. The size and morphology of the particles were examined by scanning (SEM) and transmission electron microscopy (TEM) using LEO 906E, JOEL EM100 CX and LEO 1420 microscopes. Infrared (FT-IR) spectra were recorded on an AVATAR FTIR-330 Fourier transform spectrometer supplied with a Smart Diffuse Reflectance accessory in the wavenumber (ν) range of 400–4000 cm^{-1}. The magnetic characteristics of the nanomaterials including saturation magnetization M_s were measured using a Cryogen Free Measurement System by Cryogenic Ltd (T = 7–300 K, H_{max} = 18 T). Magnetic moment per formula unit was calculated using the formula $\mu = \frac{M_s \times W}{N_A \times \mu_B}$, where M_s is saturation magnetization (emu/g), W is molar mass of the ferrite, N_A is Avogadro number and μ_B is Bohr magneton. Taking into account that magnetic moment of the formula unit is determined by Fe^{3+} ions only and magnetic moment of Fe^{3+} equals 5 μ_B, the inversion degree in ferrites was calculated as follows: $i = 1-\frac{\mu}{10\mu_B}$.

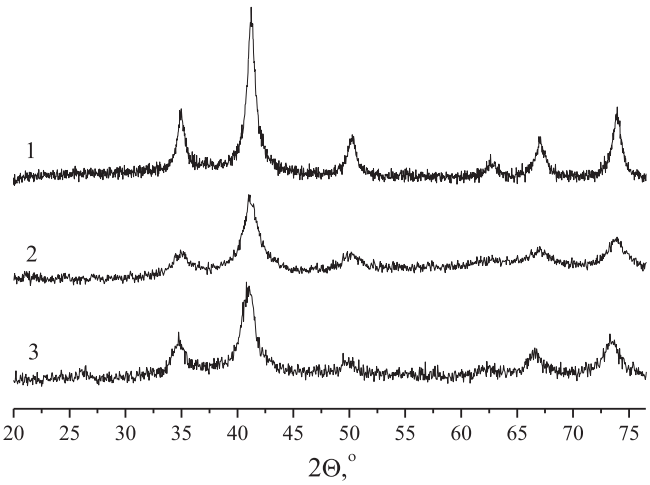

Fig. 1. Comparison of XRD patterns of $Mg_{0.5}Zn_{0.5}Fe_2O_4$ powders prepared by citrate autocombustion *(1)*, spray pyrolysis *(2)* and co-precipitation *(3)* methods.

3. Results and discussion

The XRD patterns of $Mg_xZn_{1-x}Fe_2O_4$ (x = 0.25; 0.5; 0.7) nanopowders confirm the formation of a single-phase spinel structure for all the synthesis methods used in the work. The typical patterns (on the example of the samples with x = 0.5) are shown in Fig. 1. Broad and diffuse diffraction lines observed for co-precipitation and pyrolysis methods are typical of nanosized powders. The peak broadening is lower and the peak intensity is greater for the particles obtained by citrate autocombustion method due to recrystallization processes resulting in the formation of larger sized particles at higher synthesis temperatures.

The lattice parameters of all the samples calculated from the XRD data presented in Table 1 correspond well with the published data for magnesium-zinc ferrite particles [18]. The lattice parameter of $Mg_xZn_{1-x}Fe_2O_4$ ferrite rises with increasing zinc content, which is due to the difference in ionic radii of Zn^{2+} and Mg^{2+} ions (0.074 and 0.066 nm, respectively). The lattice parameter depends strongly on the synthesis method used to prepare spinel ferrite. The lowest values of the lattice parameters relate to the particles synthesized by citrate autocombustion at 300 °C, while the highest lattice parameters are observed in case of co-precipitation synthesis at 90 °C. Therefore, an increase in temperature of the reaction mixture during the nanoparticle preparation results in the decrease of lattice parameter of ferrite powder, which corresponds well with the literature data on spinel ferrites [19,20]. However, some researchers report the opposite tendency – an increase in the lattice parameters of Mg–Zn-ferrite nanoparticles after annealing at 900 °C [12]. In particular, Eltabey and Aboulfotoh Ali reported the decrease in lattice parameter of Co–Zn-ferrite nanoparticles with increasing annealing temperature up to 350 °C and increase in lattice parameter as the temperature grows further [21]. As an explanation in can be suggested, that as the temperature increases, recrystallization

Table 1
Structural and magnetic properties of $Mg_xZn_{1-x}Fe_2O_4$ nanoparticles obtained by different methods: lattice parameter *a*, saturation magnetization M_s, inversion degree *i*, and coercivity H_c.

Synthesis method	Ferrite composition	*a*, Å	7 K			298 K		
			M_s, emu/g	*i*	H_c, Oe	M_s, emu/g	*i*	H_c, Oe
Co-precipitation	$Mg_{0.25}Zn_{0.75}Fe_2O_4$	8.453	59	0.76	90	16	0.93	0
	$Mg_{0.5}Zn_{0.5}Fe_2O_4$	8.450	62	0.76	40	23	0.91	0
	$Mg_{0.7}Zn_{0.3}Fe_2O_4$	8.444	57	0.78	100	15	0.94	0
Spray pyrolysis	$Mg_{0.25}Zn_{0.75}Fe_2O_4$	8.439	56	0.77	550	23	0.90	35
	$Mg_{0.5}Zn_{0.5}Fe_2O_4$	8.420	51	0.80	400	23	0.91	50
	$Mg_{0.7}Zn_{0.3}Fe_2O_4$	8.404	–	–	–	27	0.90	80
Citrate autocombustion	$Mg_{0.25}Zn_{0.75}Fe_2O_4$	8.426	54	0.78	420	23	0.90	50
	$Mg_{0.5}Zn_{0.5}Fe_2O_4$	8.410	74	0.71	250	30	0.86	80
	$Mg_{0.7}Zn_{0.3}Fe_2O_4$	8.394	41	0.84	300	29	0.89	80

occurs and the lattice parameter decreases as the defects vanish from the lattice. However, the role of cation redistribution between *A*- and *B*-sites of the lattice increases at higher temperatures, which may cause an increase in the lattice parameter.

For the samples obtained by spray pyrolysis, the lattice parameter value lies in-between, although the temperature in the reaction zone is higher (650 °C) than in case of the other methods mentioned above. However, a short heat treatment time in this case does not allow achieving significant cation redistribution between sublattices.

The calculation of the crystallite size based on the diffraction reflection broadening showed insignificant differences in the size for powders of different compositions obtained by the same method. The average crystallite size was found to be ~15 nm for the particles prepared by co-precipitation, ~10 nm for pyrolysis and ~25 nm for citrate autocombustion method. For all the methods, a slight decrease in the size of the nanoparticles with increasing zinc content was observed.

Infrared spectroscopy was used to reveal the structural peculiarities of the prepared materials that could not be acquired by XRD method. Fig. 2 displays a typical FT-IR spectra of ferrite powders with the same composition ($Mg_{0.5}Zn_{0.5}Fe_2O_4$) obtained by different methods. In the characteristic range (400 ÷ 1000 cm^{-1}), all the spectra contain absorption bands with a maximum intensity at ~550 cm^{-1} (ν_1) and ~430 cm^{-1} (ν_2), which is typical of spinel-type structure. These bands are associated with *Me*–O stretching vibrations in tetrahedral and octahedral positions, respectively. An important feature of the spectra is the difference in relative intensities of ν_1 and ν_2 bands for the samples obtained by different methods. In case of the ferrites prepared by citrate autocombustion, the intensity of ν_1 corresponding to O–Me_{tetr} is greater than ν_2(O–Me_{oct}). On the contrary, the samples synthesized by spray pyrolysis and co-precipitation demonstrate the opposite intensity ratio. This proves the structural changes associated with different cation distribution in case of high and lower temperature synthesis. The same structural changes were observed for nickel ferrite particles with different size indicating the structure transition from normal to inverse spinel with the increase in particle size [22].

Also, the IR spectra contain bands around 900 cm^{-1} reflecting bending vibrations of OH-groups chemically linked with metal cations, δ(*Me*–OH). A pronounced band at 918 cm^{-1} is found in case of the precipitation-derived sample, while the other spectra contain only minor peaks. This is evidently related to the temperature of the synthesis. Thus, co-precipitation approach assumed a low temperature processing (90 °C) as compared to citrate autocombustion (at least 300 °C) and spray pyrolysis (650 °C). A high concentration of structural OH-groups is typical of chemical co-precipitation method since the low temperature of the synthesis does not stimulate effective dehydration processes.

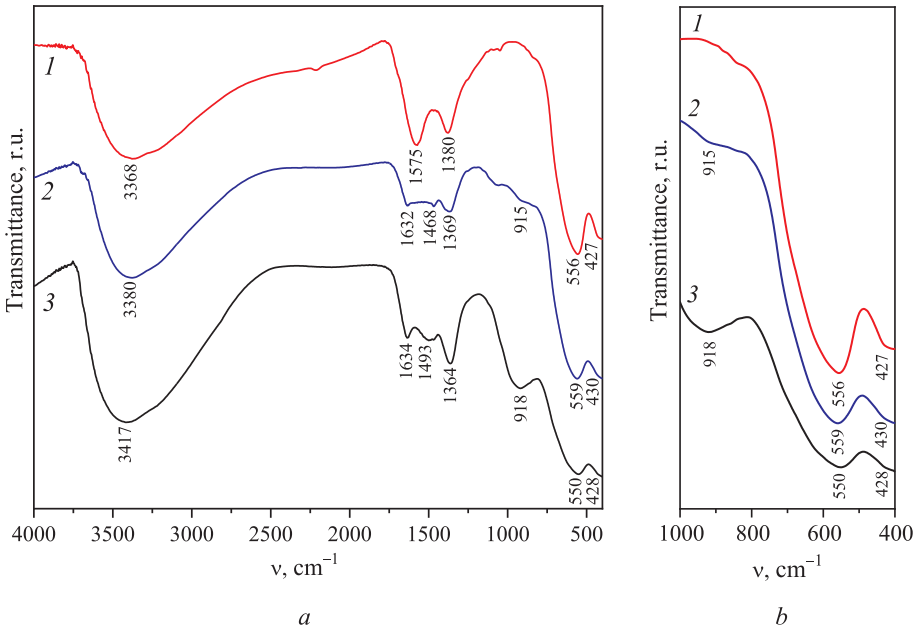

Fig. 2. Overview (*a*) and characteristic groups region (*b*) of IR spectra of $Mg_{0.5}Zn_{0.5}Fe_2O_4$ nanoparticles obtained by different methods: *1* – citrate autocombustion synthesis; *2* – spray pyrolysis; *3* – co-precipitation.

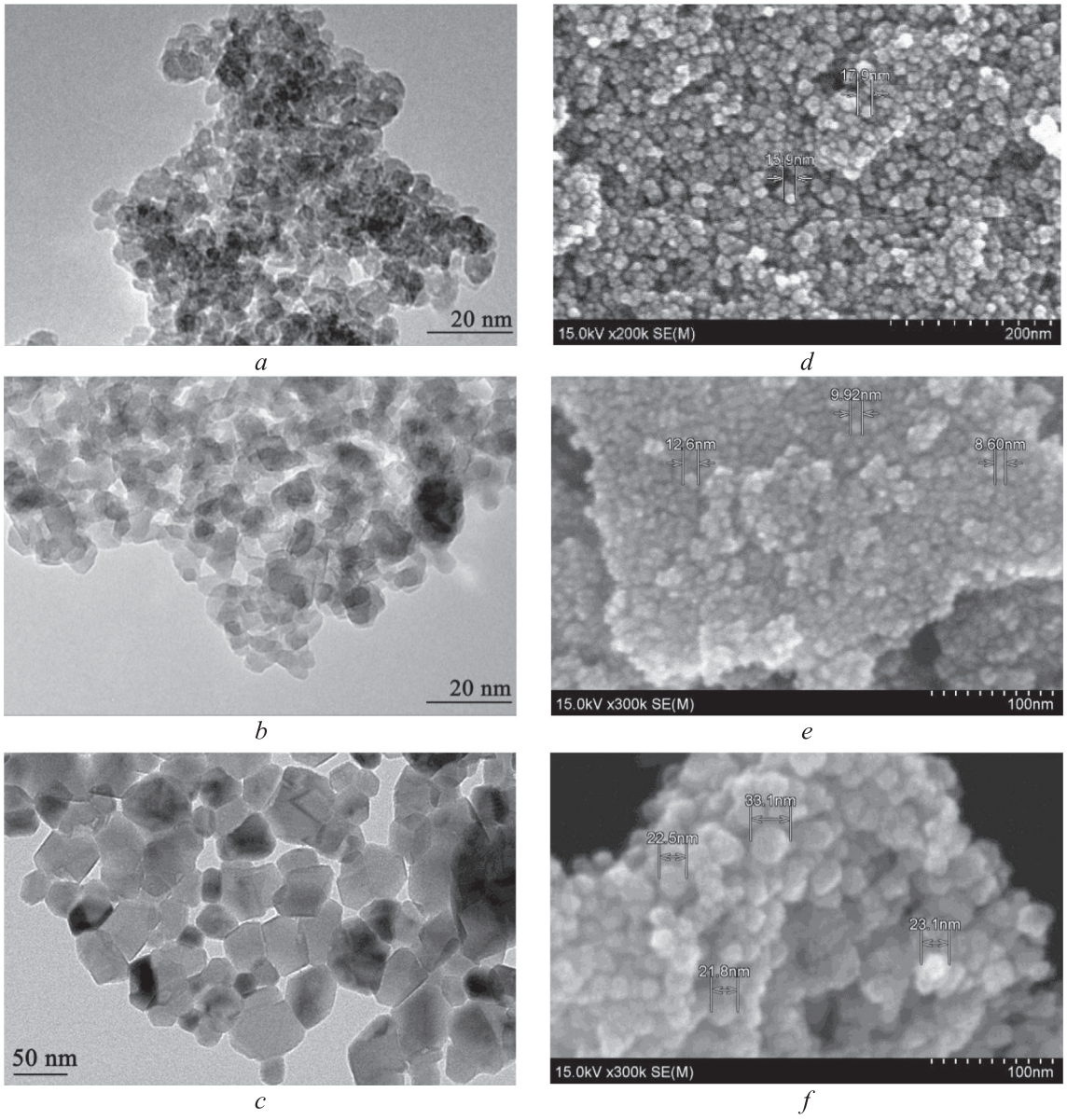

Fig. 3. TEM micrographs of $Mg_{0.7}Zn_{0.3}Fe_2O_4$ (*a–c*) and SEM micrographs of $Mg_{0.5}Zn_{0.5}Fe_2O_4$ *(d–f)* nanoparticles prepared by co-precipitation (*a*, *d*), spray pyrolysis (*b*, *e*) and autocombustion (*c*, *f*).

The same speculations are valid for water adsorbed at the surface of the materials. The relative intensities of bands around 3400 cm^{-1} and 1600 cm^{-1} assigned to stretching and bending vibrations of O—H bonds confirm the higher degree of hydration of co-precipitated samples. Nevertheless, the samples obtained by all three approaches are characterized by highly hydrophilic surface. This is important for applications where further modification of the particles and their stabilization in form of aqueous dispersions are required.

The particle size, agglomeration degree and size distribution were studied by scanning and transmission electron microscopy. Fig. 3 shows the images of nanoparticles obtained by different methods. The corresponding grain size distribution histograms are given in Fig. 4. It is seen that co-precipitation method is characterized by a formation of highly dispersed nanoparticles with a particle size of ~10 nm, which corresponds well with the particle size calculated from the XRD data. Due to the use of a relatively low-temperature synthesis method, no aggregation of nanoparticles occurs during their formation. When dried, the particles form a highly porous aerated structure, which subsequently easily collapses to form colloidal solutions. In the TEM images of the co-precipitated samples, it is possible to observe individual crystallographic planes of the grains, which indicates their crystalline nature at nano-scale level.

Citrate autocombustion method is characterized by the formation of larger particles (the main fraction is 40–70 nm) sintered into stable aggregates with phase contacts between grains. To eliminate the aggregation, the introduction of an inert component (NaCl) in the solution of precursors is proposed. The presence of NaCl is meant to facilitate the spatial separation of particles during the synthesis and further heat treatment. Subsequently, upon removal of the inert component after recrystallization, it is possible to obtain non-agglomerated facetted nanoparticles (Fig. 3 c) with a wide size distribution (15–100 nm).

The classical method of spray pyrolysis also implies the formation of aggregates of nanoparticles, even despite the short duration of exposure to high temperatures. To prevent aggregation, the same as for nitrate-citrate method, NaCl was added to the solution before spraying. This allows not only preventing the aggregation, but also limiting the growth of nanoparticles. The size of the nanoparticles obtained by the pyrolysis method lies in the range of 10–20 nm. It can be easily controlled by

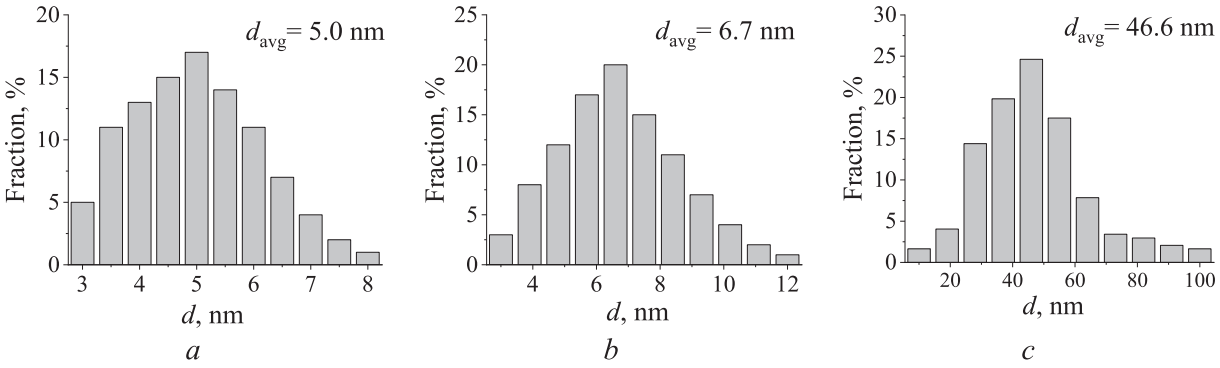

Fig. 4. Grain size distribution of $Mg_{0.7}Zn_{0.3}Fe_2O_4$ powders prepared by co-precipitation (*a*), spray pyrolysis (*b*) and autocombustion (*c*) methods plotted according to the TEM data.

changing the pyrolysis parameters, such as temperature, solution composition and concentration, flow rate of the carrier gas, etc.

To compare the magnetic properties of $Mg_xZn_{1-x}Fe_2O_4$ ferrite nanoparticles, the saturation magnetization, coercivity and inversion degree of the spinel calculated from saturation magnetization value were chosen. Fig. 5 represents specific magnetization curves of the samples recorded at 7 and 298 K. At 7 K, all the samples studied demonstrate hysteresis behavior with coercivities of 50–100 Oe (co-precipitation), 250–450 Oe (citrate autocombustion) and 400–600 Oe (spray pyrolysis).

At room temperature, all the particles synthesized by co-precipitation are in superparamagnetic state, as there is no hysteresis loop on the magnetization curves and specific magnetization does not reach saturation up to 50 000 Oe. As for the particles obtained by spray pyrolysis and citrate autocombustion method, hysteresis behavior with small coercivities (40–80 Oe) is observed at room temperature. The presence of coercivity for the samples synthesized at higher temperatures can be related to the increase in particle size.

As the particle size increases approaching the critical value for single-domain structure, the coercivity grows as well due to the decrease in thermal fluctuations role in disorientation of magnetic spins. The critical value of such transition for magnetite and magnesium ferrite is about 20 nm [23,24], which corresponds quite well with our results for Mg–Zn-ferrites. In case of citrate autocombustion synthesis, the average particle size grows up to ~40–50 nm, and the hysteresis loop appears on magnetization curves. For the nanoparticles prepared by spray pyrolysis, the average particle size is lower (~20 nm), however, the presence of the fraction with bigger particle size provides the existence of hysteresis.

Among the studied compositions, the highest saturation magnetization at room temperature corresponds to ferrites obtained using citrate combustion synthesis. This can be explained by the differences in cation distribution attributed to different synthesis methods. With the increase in treatment temperature, the inversion degree in spinel ferrites is known to decrease to 2/3, which corresponds to a random cation distribution over spinel sublattices [25]. Therefore, a relatively low inversion degree could be expected for high synthesis temperatures, which would result in higher saturation magnetization values. Here, the saturation magnetization of the ferrites obtained by citrate autocombustion method (synthesis temperature ~300 °C) exceeds significantly the saturation magnetization value of the particles prepared by co-precipitation (90 °C). The nanoparticles obtained by pyrolysis possess intermediate values of the saturation magnetization, despite the highest (600 °C) synthesis temperature. This is due to the short time for the aerosols to pass through the high-temperature reaction zone (~1–2 s), when there is not enough time for the considerable redistribution of ions between the sublattices. This phenomenon is of the same nature as the lattice parameter dependence on the temperature described earlier. As the synthesis temperature rises, the cation redistribution takes place, which results in changes of the lattice parameter and saturation magnetization of the material.

The values of inversion degree of spinel ferrites obtained by different methods calculated from the specific magnetization values are given in Table 1. The lowest inversion degrees and, therefore, the highest saturation magnetization values at room temperature relate to the ferrite particles prepared by citrate autocombustion synthesis. The highest inversion degree is observed in case of co-precipitation synthesis, whilst the use of spray pyrolysis method leads to intermediate values.

However, at low temperature, the inversion degree of the ferrites synthesized by coprecipitation does not exceed the magnitudes measured for ferrites obtained by other methods. For example, in case of $Mg_{0.5}Zn_{0.5}Fe_2O_4$ nanoparticles, the highest inversion degree value at 7 K is observed for spray pyrolysis synthesis, and in case of $Mg_{0.25}Zn_{0.75}Fe_2O_4$ the particles obtained by co-precipitation exhibit the highest saturation magnetization (see Fig. 5). To explain this, the role of surface magnetically disordered spin layer, which causes the decrease in saturation magnetization of nanoparticles as compared to bulk materials, should be considered. El-Sayed et al. calculated the thickness of the defective layer in $Mg_xZn_{1-x}Fe_2O_4$ system to be ~1 nm for the particles with an average size of 10 nm [26]. According to the theory proposed by De Biasi et al., ferromagnetic clusters can be formed in the shell layer of magnetic particle at low temperature causing an increase in magnetic moment and saturation magnetization [27]. With the decrease in particle size the contribution of surface layer to specific magnetization of the particle increases, therefore, the increase in magnetization at low temperature is the most significant for the smallest particles. Singh et al. noted that the growth of magnetic core size in Mn–Zn-ferrites causes less interactions between surface magnetic moments and, therefore, leads to a drop of saturation magnetization at low temperature [28]. This idea also explains the abnormally low saturation magnetization of $Mg_{0.7}Zn_{0.3}Fe_2O_4$ prepared by citrate autocombustion at 7 K.

The dependence of the saturation magnetization on the composition of ferrite particles given in Table 1 is non-linear. For the mixed ferrites obtained by citrate autocombustion and co-precipitation methods, the maximum saturation magnetization at both room and low temperatures corresponds to $Mg_{0.5}Zn_{0.5}Fe_2O_4$ sample with Mg and Zn content intermediate between $Mg_{0.7}Zn_{0.3}Fe_2O_4$ and $Mg_{0.25}Zn_{0.75}Fe_2O_4$ compositions.

Magnesium ions are known to occupy preferably octahedral positions in ferrite spinel lattice, with Fe^{3+} ions being displaced to tetrahedral sites. As a result, the specific magnetization of ferrite decreases due to a compensation of magnetic moments of Fe^{3+} ions in tetra- and octahedral sublattices. In contrast, zinc ions tend to occupy predominantly tetrahedral positions in the crystal lattice, causing the transition of some iron ions to octahedral sites and the formation of inverse spinel structure. Therefore, as the content of zinc increases up to

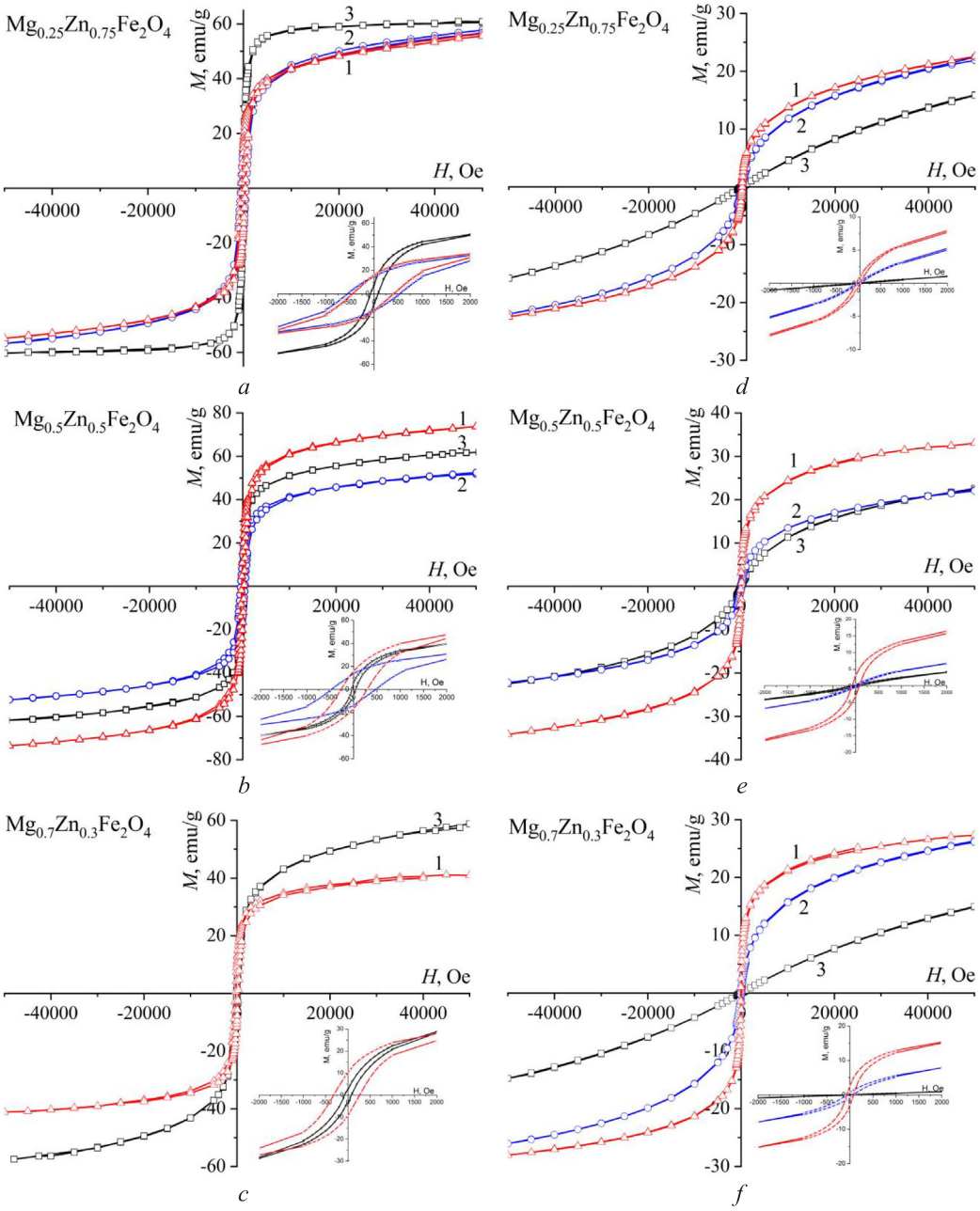

Fig. 5. Specific magnetization curves of $Mg_xZn_{1-x}Fe_2O_4$ powders obtained by different methods at 7 K (*a, b ,c*) and 298 K (*d, e, f*): *1* – citrate autocombustion synthesis; *2* – spray pyrolysis; *3* – co-precipitation. The hysteresis loops recorded at low field are on insert graphs.

some limit, the specific magnetization increases as well [29]. However, for high zinc contents, Zn^{2+} ions start to shift from tetra- to octahedral positions, and the specific magnetization of the material decreases. Therefore, the highest saturation magnetization for different ferrite compositions obtained by citrate autocombustion and co-precipitation methods corresponds to the optimal zinc content and the lowest inversion degree.

For the nanoparticles synthesized by spray pyrolysis method, the inversion degree at room temperature is almost constant with little relation to the ferrite composition. A possible explanation of this effect is in a short time of the precursor solution exposure to high temperature in the reaction zone. Therefore, the product phase is rapidly formed from a solution droplet, and a random ion distribution occurring in the precursor solution remains in the product particles. When zinc content is comparatively low ($Mg_{0.7}Zn_{0.3}Fe_2O_4$), the spinel structure with most of zinc ions locating in tetrahedral sites of the lattice is formed. With increasing zinc content ($Mg_{0.5}Zn_{0.5}Fe_2O_4$ and $Mg_{0.3}Zn_{0.7}Fe_2O_4$), as the solid fraction is formed during solvent evaporation, there is lack of time for all zinc ions to shift to tetrahedral sites, and some of them remain in octahedral sites in accordance with their initial positions in the system. As a result, the amount of Fe^{3+} ions in the octa-positions decreases, which leads to the drop of specific magnetization of the material. The opposite effect can be observed in case of magnesium ions. Thus, despite the high affinity of magnesium ions for octa-positions, some of them remain in tetra-sublattice in $Mg_{0.7}Zn_{0.3}Fe_2O_4$, causing the specific magnetization to increase as compared to the compositions with lower magnesium content. A lower concentration of magnesium content in the precursor solution causes the growth of their content in octa-

positions. Thus, an equilibrium is established, and the inversion degree practically does not change for different compositions, which explains the small difference between specific magnetization values for spray pyrolysis synthesis.

4. Conclusions

Magnetic ferrite nanoparticles with the composition of $Mg_xZn_{1-x}Fe_2O_4$ ($x = 0.25, 0.5, 0.7$) were synthesized by co-precipitation, spray pyrolysis and citrate autocombustion method. The procedures that allow obtaining single-phased products with a spinel-type crystal lattice were elaborated for each of the techniques used. The influence of the synthesis conditions, namely the temperature and duration of heat treatment on the magnetic characteristics of the nanopowders was revealed. Using co-precipitation method, superparamagnetic nanoparticles with a low crystallization degree, average diameter of ~10 nm and narrow size distribution were formed. Increasing synthesis temperature leads to the growth of particle size (40–70 nm for spray pyrolysis and 20–90 nm for citrate autocombustion), broadening the particle size distribution and the occurrence of coercivity (30–80 Oe) at room temperature. Moreover, higher temperatures and longer thermal treatment were found to lead to the cation redistribution between spinel sublattices, which results in an increase of the specific magnetization of the materials. At room temperature, the ferrites obtained by citrate autocombustion method show the highest specific magnetization values and the lowest inversion degree values. At 7 K, however, the specific magnetization of the co-precipitation products increases significantly as compared to the samples synthesized by other methods, which may be due to a higher contribution of surface layer in case of smaller particles. The magnetic properties of the materials show non-linear dependence on the Zn content. In case of citrate autocombustion and coprecipitation methods, the magnetization goes through a maximum at $Mg_{0.5}Zn_{0.5}Fe_2O_4$, whereas the dependence on the composition is subtle for spray pyrolysis. The highest specific magnetization at both 7 and 298 K relates to $Mg_{0.5}Zn_{0.5}Fe_2O_4$ nanopowders prepared by citrate autocombustion method (74 and 30 emu/g, respectively).

References

[1] L. Mohammed, H.G. Gomaa, D. Ragab, J. Zhu, Magnetic nanoparticles for environmental and biomedical applications: a review, Particuology 30 (2017) 1–14.
[2] T. Tatarchuk, M. Bououdina, J. Judith Vijaya, L. John Kennedy, Spinel Ferrite Nanoparticles: Synthesis, Crystal Structure, Properties, and Perspective Applications, in: O. Fesenko, L. Yatsenko (Eds.), Nanophysics, Nanomaterials, Interface Studies, and Applications, Springer Proceedings in Physics, 2017, pp. 305–325.
[3] I. Matsui, Nanoparticles for electronic device applications: A brief review, J. Chem. Eng. Jpn. 38 (2005) 535–546.
[4] I. Koh, L. Josephson, Magnetic nanoparticle sensors, Sensors 9 (2009) 8130–8145.
[5] A. Daigle, et al., Structure, morphology and magnetic properties of $Mg_{(x)}Zn_{(1-x)}Fe_2O_4$ ferrites prepared by polyol and aqueous co-precipitation methods: a low-toxicity alternative to $Ni_{(x)}Zn_{(1-x)}Fe_2O_4$ ferrites, Nanotechnology 22 (2011) 305708–305714.
[6] Yu.V. Bogachev, et al., NMR relaxation efficiency of aqueous solutions of composite $Mg_xZn_yFe_{3-x-y}O_4$ nanoparticles, Appl. Magn. Reson. 48 (2017) 715–722.
[7] P. Reyes-Rodriguez, et al., Structural and magnetic properties of Mg-Zn ferrites ($Mg_{1-x}Zn_xFe_2O_4$) prepared by sol-gel method, J. Magn. Magn. Mater. 427 (2017) 268–271.
[8] S. Ounnunkad, P. Winotai, S. Phanichphant, Cation distribution and magnetic behavior of $Mg_{1-x}Zn_xFe_2O_4$ ceramics monitored by Mössbauer Spectroscopy, J. Electroceram. 16 (2006) 363–368.
[9] S.W. Da Silva, et al., Effect of the Zn content in the structural and magnetic properties of $Zn_xMg_{1-x}Fe_2O_4$ mixed ferrites monitored by Raman and Mössbauer spectroscopies, J. Appl. Phys. 107 (2010) 09B503.
[10] A.M. Gismelseed, et al., Structure and magnetic properties of the $Zn_xMg_{1-x}Fe_2O_4$ ferrites, J. Phys.: Conf. Ser. 217 (2010) 012138.
[11] T. Tatarchuk, et al., Structural, optical and magnetic properties of Zn-doped $CoFe_2O_4$ nanoparticles, Nanoscale Res. Lett. 12 (2017) 141–151.
[12] K. Nadeem, S. Rahman, M. Mumtaz, ffect of annealing on properties of Mg doped Zn-ferrite nanoparticles, Prog. Nat. Sci.: Mater. Int. 25 (2015) 111–116.
[13] S.S. Khot, et al., Magnetic and structural properties of magnesium zinc ferrites synthesized at different temperature, Adv. Appl. Sci. Res. 2 (2011) 460–471.
[14] C. Choodamani, et al., Structural and magnetic studies of $Mg_{(1-x)}Zn_xFe_2O_4$ nanoparticles prepared by a solution combustion method, J. Alloys Compd. 578 (2013) 103–109.
[15] G.F. Barbosa, et al., Enhanced magnetic properties of Zn substituted Mg ferrite, IEEE Trans. Magn. 49 (2013) 4562–4564.
[16] D.C. Bharti, et al., Wet chemical synthesis and gas sensing properties of magnesium zinc ferrite nano-particles, Mat. Chem. Phys. 120 (2010) 509–517.
[17] V.D. Kassabova-Zhetcheva, Characterization of the citrate precursor, used for synthesis of nanosized Mg-Zn ferrites, Cent. Eur. J. Chem. 7 (2009) 415–422.
[18] K.A. Mohammed, et al., Infrared and structural studies of $Mg_{1-x}Zn_xFe_2O_4$ ferrites, Physica B 407 (2012) 795–804.
[19] Ch. Srinivas, et al., Superparamagnetic behavior of heat treated $Mg_{0.5}Zn_{0.5}Fe_2O_4$ ferrite nanoparticles studied by Mössbauer spectroscopy, AIP Conf. Proc. 1731 (2016) 050074.
[20] M. Zhang, et al., Size effects on magnetic properties of $Ni_{0.5}Zn_{0.5}Fe_2O_4$ prepared by sol-gel method, Adv. Mat. Sci. Eng., V. 2013 (2013) 10. Article ID 609819.
[21] M.M. Eltabey, Ali N. Aboulfotoh, Effect of annealing temperature on structural and magnetic properties of Co-Zn ferrite nanoparticles, Int. J. Adv. Res. 2 (2014) 184–192.
[22] J. Jacob, Khadar M. Abdul, Investigation of mixed spinel structure of nanostructured nickel ferrite, J. Appl. Phys. 107 (2010) 114310.
[23] J. Baumgartner, L. Bertinetti, M. Widdrat, A.M. Hirt, D. Faivre, Formation of magnetite nanoparticles at low temperature: from superparamagnetic to stable single domain particles, PLoS One 8 (2013) e57070.
[24] T. Sasaki, et al., Continuous synthesis of fine $MgFe_2O_4$ nanoparticles by supercritical hydrothermal reaction, J. Supercrit. Fluids 53 (2010) 92–94.
[25] H.S.C. O'Neill, A. Navrotsky, Simple spinels: crystallographic parameters, cation radii, lattice energies and cation distribution, Amer. Mineralog. 68 (1983) 181–194.
[26] H.M. El-Sayed, I.A. Ali, A. Azzam, A.A. Sattar, Influence of the magnetic dead layer thickness of Mg-Zn ferrites nanoparticle on their magnetic properties, J. Magn. Magn. Mater. 424 (2017) 226–232.
[27] E. De Biasi, C.A. Ramos, R.D. Zysler, H. Romero, Large surface magnetic contribution in amorphous ferromagnetic nanoparticles, Phys. Rew. B. 65 (2002) 144416.
[28] S.B. Singh, Ch. Srinivas, et al., Structural, thermal and magnetic studies of $Mg_xZn_{1-x}Fe_2O_4$ nanoferrites: Study of exchange interactions on magnetic anisotropy, Ceram. Int. 42 (2016) 19179–19186.
[29] V.S. Bushkova, Synthesis and study of the properties of nanoferrites obtained by the sol-gel method with participation of auto-combustion, J. Nano- Electron. Phys. 7 (2015) 01023.